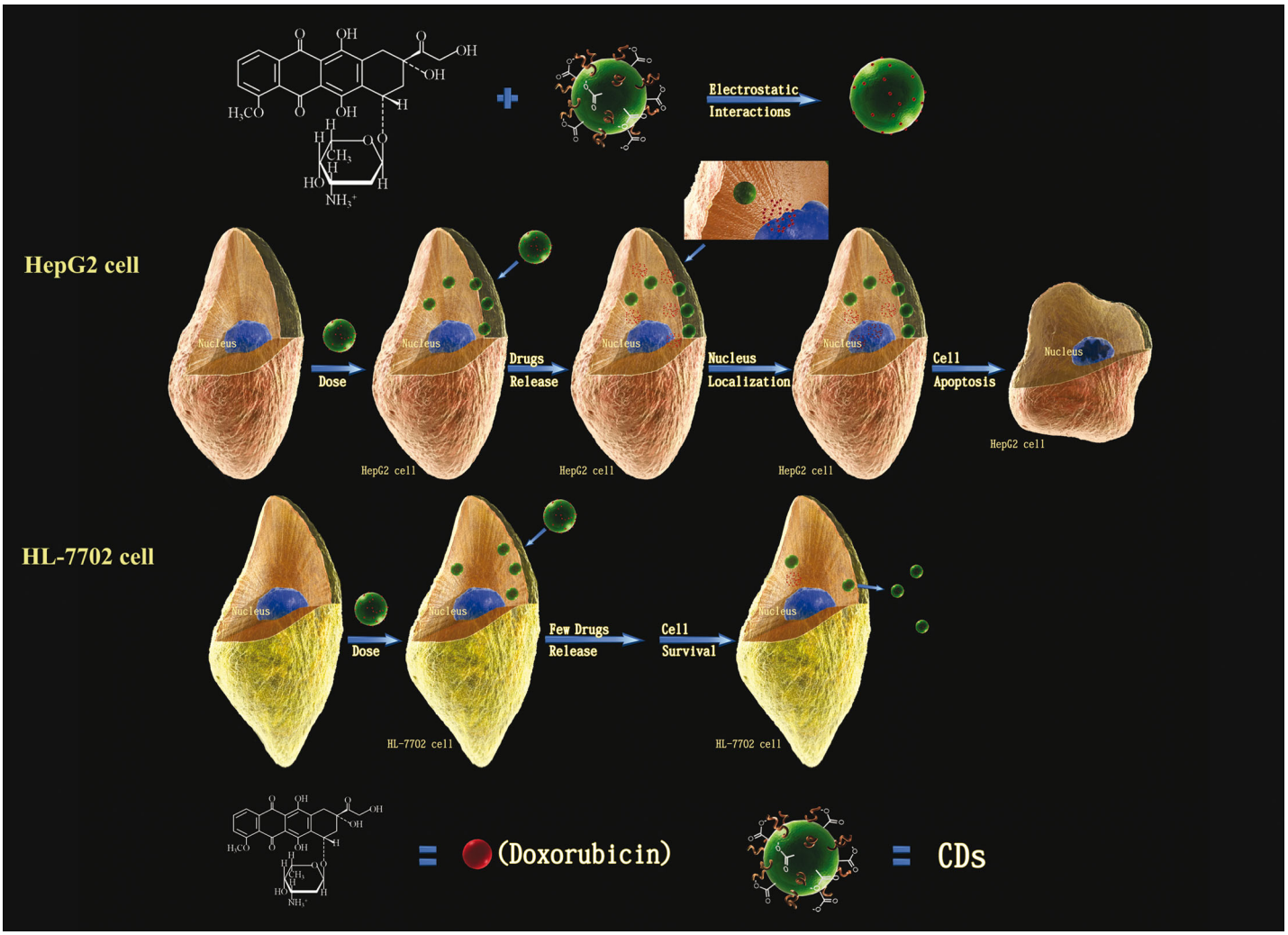

Highlighting research from the State Key Laboratory of Luminescence and Applications, Changchun Institute of Optics, Fine Mechanics and Physics, Chinese Academy of Sciences, China.

Carbon dots as a trackable drug delivery carrier for localized cancer therapy *in vivo*

The green carbon dots with carboxyl-rich surfaces were employed as a selective nanocarrier for fluorescent traceable and pH-sensitive doxorubicin delivery in localized cancer treatment.

As featured in:

See Chongxin Shan, Jing Li, Qin Li *et al.*, *J. Mater. Chem. B*, 2016, **4**, 5119.

ROYAL SOCIETY OF CHEMISTRY

www.rsc.org/MaterialsB

Registered charity number: 207890

Journal of Materials Chemistry B

PAPER

View Article Online
View Journal | View Issue

Cite this: J. Mater. Chem. B, 2016, 4, 5119

Carbon dots as a trackable drug delivery carrier for localized cancer therapy *in vivo*†

Qinghui Zeng,‡[a] Dan Shao,‡[b] Xu He,‡[c] Zhongyuan Ren,[a] Wenyu Ji,[a] Chongxin Shan,*[a] Songnan Qu,[a] Jing Li,*[b] Li Chen[b] and Qin Li*[d]

Received 19th May 2016,
Accepted 27th June 2016

DOI: 10.1039/c6tb01259k

www.rsc.org/MaterialsB

Fluorescent carbon dots (CDs) with a size smaller than 10 nm, excellent biocompatibility, and low to no cytotoxicity are considered as a rising star in nanomedicine. In this report, for the first time we demonstrate that green-emitting CDs with a carboxyl-rich surface can be employed as a trackable drug delivery agent for localized cancer treatment in a mouse model. The CDs are conjugated with the cancer drug, Doxorubicin (DOX), *via* non-covalent bonding, utilizing the native carboxyl groups on CDs and the amine moiety on DOX molecules. The pH difference between cancer and normal cells was successfully exploited as the triggering mechanism for DOX release. Our *in vivo* study demonstrated that the fluorescent CDs can serve as a targeted drug delivery system for localized therapy, and the stimuli-responsive non-covalent bonding between the nanodot carrier and the drug molecule is sufficiently stable in complex biological systems. Taken together, our work provides a strategy to promote the potential clinical application of CDs in cancer theranostics.

Introduction

Targeted drug delivery, localised disease treatment, and personalised cures are the ultimate goals in modern medicine. Such a development relies on precise biochemical fundamental understandings and equally importantly, observable biochemical activity reporters.[1] In current cancer treatment, chemotherapy is still regarded as the most effective method, which, as widely known, causes significant side effects to patients, because of its non-discriminating destructive impact on both cancer and normal cells. The significant challenge in cancer chemotherapy and most complex diseases is to understand the drug distribution within the organs and to devise a selective drug release system targeted at cancer cells.[2,3] Therefore, developing sophisticated strategies to achieve both targeted and traceable anti-cancer drug delivery is of critical importance.

Recent years have seen increased activities in developing multifunctional nanomaterials that can enable bioimaging, disease detection and drug delivery simultaneously. Various nanoparticles (NPs), including gold NPs,[4–6] iron oxide NPs,[7–10] semiconductor quantum dots (QDs),[11,12] polymer NPs,[13–16] carbon NPs,[17,18] and graphene,[19] have been explored as potential candidates for integrating different functions. It should be appreciated that the design and application of these multifunctional therapeutic nanoformulations need to be intimately linked with physiological parameters.

Fluorescent carbon dots (CDs) with a size smaller than 10 nm, excellent biocompatibility, low to no cytotoxicity, high quantum yield, non-blinking character, and low cost[20–26] are considered as a rising star in nanomedicine. However, in terms of emission tunability, the control over the emission of CDs is still in progress with increased understanding of the interplay between the surface states and intrinsic states in photoluminescence.[27–30] Recent developments have yielded a simple synthesis of highly green-emitting CDs[20] and red-emitting CDs,[31] which qualifies CDs as an *in vivo* bioimaging agent. However, in terms of CDs' potential as a trackable drug delivery system *in vivo*, there have been limited reports to date.[18]

In this work, we engineered green-emitting CDs synthesized by a simple one-step microwave synthesis[20] into a drug delivery system that discriminates cancer cells from normal cells. Inspired by previous studies,[32,33] we utilize the difference of pH between cancer and normal tissue as the motif for designing cancer-specific drug delivery. Liver cancer is chosen as the target disease, because it is the third leading cause of cancer-related human death worldwide with a fast increasing trend in incidence rate (>600 000 new incidents per year).[34] Doxorubicin (DOX), as a broad-spectrum anticancer agent, was selected as the model drug

[a] State Key Laboratory of Luminescence and Applications, Changchun Institute of Optics, Fine Mechanics and Physics, Chinese Academy of Sciences, Dong_Nanhu Road 3888, Changchun 130033, China. E-mail: shancx@ciomp.ac.cn
[b] Department of Pharmacology, College of Basic Medical Sciences, Jilin University, Changchun, P. R. China. E-mail: lijing@jlu.edu.cn
[c] The Key Laboratory of Pathobiology, Ministry of Education, College of Basic Medical Sciences, Jilin University, Changchun, P. R. China
[d] Queensland Micro- and Nanotechnology Centre & Environmental Engineering, Griffith University, Brisbane, QLD 4111, Australia. E-mail: qin.li@griffith.edu.au

† Electronic supplementary information (ESI) available: Fig. S1–S4. See DOI: 10.1039/c6tb01259k

‡ These authors contributed equally to this work.

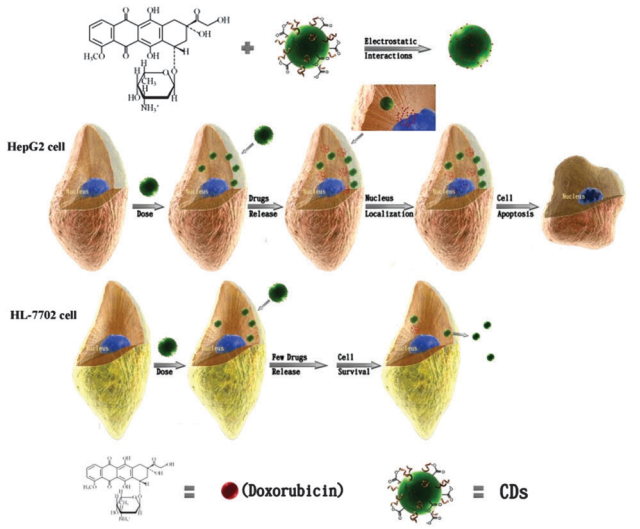

Fig. 1 Schematic illustration of the experimental design overview. (a) The amines ($-NH_2$) on DOX bind with the carboxylic acid (–COOH) on CDs *via* electrostatic interactions or hydrogen bonding. (b) Delivery of CD–DOX conjugates to HepG2 cancer cells and HL-7702 normal cells with strong green signal imaging tracking. The CD–DOX conjugates are expected to release DOX in HepG2 cancer cells, but not HL-7702 normal liver cells, due to low pH in cancer cells.

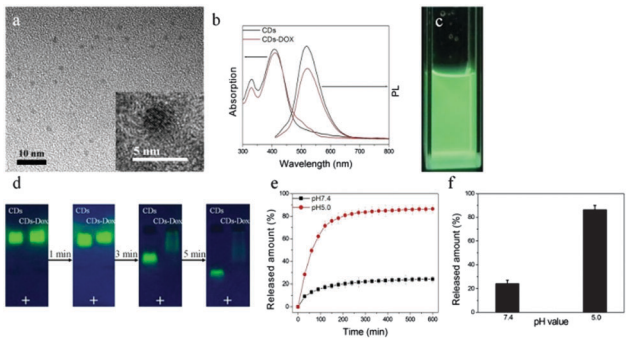

Fig. 2 (a) TEM and HRTEM (inset) images of the CDs, scale bar indicates 10 nm. (b) Absorption and PL spectrum of CDs and CD–DOX conjugates. (c) A photo of CDs under an UV lamp. (d) Digital photo of the agar gel electrophoresis of CDs and CD–DOX during different electrophoresis times under a 365 nm ultraviolet lamp. '+' indicates the positive pole of the electrophoresis. (e) pH-dependence of the released quantity of DOX from the CD–DOX nanocomposites. (f) Released amounts of DOX from the CD–DOX nanocomposites at pH 5.0 and 7.4 after 10 hours.

agent in our study.[35] In this study, we show that the as-synthesized CDs and DOX can form conjugates simply by non-covalent bonding (electrostatic interactions or *via* hydrogen bonds) between the –COOH group on CDs and the $-NH_2$ group on DOX. This bonding method is sensitive to environmental pH, hence can be employed as the manipulating strategy for cancer-specific localized drug release (as illustrated in Fig. 1). We carried out a series of *in vitro* and *in vivo* studies and demonstrated that carboxyl-rich green-emitting CDs are nontoxic bioimaging agents for drug biodistribution research, and more significantly for the first time we demonstrated an *in vivo* study showing that the CDs can be used as a stable cancer drug delivery system that can selectively kill cancer cells performing localized therapy owing to their finite size and rich surface chemistry for forming non-covalent bonds with drug payloads.

Results and discussion

Synthesis, characterization and pH-dependent DOX release of CD–DOX conjugates

The morphology of the microwave synthesized CDs[20] was analyzed by transmission electron microscopy (TEM) measurements (Fig. 2a). The CDs appear spherical and well dispersed, with a size ranging from 2 to 6 nm. Further from the inset of Fig. 2a, it can be calculated that the interplanar spacing of the CDs is around 0.32 nm. With a urea to citric acid molar ratio of 2 : 1, the as-prepared CDs have predominantly carboxylic acid (–COOH) groups on the surface,[20] unlike CDs synthesized with other urea to citric acid ratios that usually have predominantly amine ($-NH_2$) groups on the surface.[18,27,36] Therefore, our as-prepared CDs can favorably interact with the amine ($-NH_2$) moiety of DOX *via* electrostatic attraction as shown in the experimental design overview in Fig. 1.

The as-prepared CDs show intense green fluorescence under a UV lamp as shown in Fig. 2c. The UV-vis absorption of both CDs and CD–DOX nanoformulation shows a clear band at 409 nm from the π–π conjugated structure, and a strong photoluminescence (PL) peak centered at 518 nm, as shown in Fig. 2b. The PL quantum yield of the as-prepared CDs is 36%. It can be observed from Fig. 2b that there is a small absorption peak centered around 480 nm in the UV-vis, and an almost negligible shoulder around 590 nm in the PL spectrum after the combination with DOX, which is due to the absorption and emission of DOX molecules (shown in Fig. S1, ESI†). Both of those CDs and CD–DOX conjugates are stable in water suspension for several months without changes in their optical properties. It should be noted that in this study there is no noticeable energy transfer between CDs and DOX as shown in Fig. 2b. The absorbance peak of DOX appears at 480 nm, and the fluorescence peak of CDs appears at 518 nm. The mismatch of the donor and acceptor maxima does not appear to support an obvious fluorescence resonance energy transfer process from CDs to DOX. We drew this conclusion from the changeless PL spectra before and after the CDs were bonded with DOX as shown in Fig. 2b, where the decrease of the PL intensity was mainly due to the decrease of the absorption of CDs.

Gel electrophoresis was employed to confirm the binding of CDs and DOX at pH 7, as shown in Fig. 2d. Green fluorescence of CDs and CD labeled DOX are observed under the excitation of an ultraviolet lamp. Because of the non-covalent bonding between the $-COO^-$ group on the CDs and the $-NH_2$ moiety on DOX, the surface charge of the CDs was neutralized, leading to a lower total surface charge of the CD–DOX nanoformulation compared to CDs alone. Therefore, the CD–DOX migrated significantly slower than CDs alone and separated well in 0.8% agar gel electrophoresis, which is unambiguous evidence demonstrating the successful binding of CDs and DOX.

To investigate the pH-triggered release of this CD–DOX nanoformulation, the same quantity of CD–DOX was immersed in phosphate buffer at different pHs. Fig. 2e shows the pH-dependence of the released amount for DOX *versus* time at a pH of 5.0 and 7.4, respectively. Notably, the released amount of DOX was significantly lower at pH 7.4, whereas at pH 5.0, there was a steady release over about 6 h, proving that drug release in this CD–DOX conjugate system can be controlled effectively by pH, and DOX can be favorably released in a mild acidic environment. As can be seen in Fig. 2f, a very clear and highly effective pH-operable gating effect was demonstrated by monitoring the fluorescence of DOX (590 nm). The almost 4-fold increase of released drug from 24.2% to 86.5% by adjusting the pH from 7.4 to 5.0 demonstrates the effective stimuli-responsive performance of the CD–DOX delivery system. The pH response also shows that the binding between CDs and DOX is electrostatic in origin and facilitated by hydrogen bonding.[37] It is also possible that π–π stacking between the phenyl ring of DOX and the sp^2 domain of the CDs could play a role in the binding. It was reported that DOX becomes more water-soluble in an acidic environment, which could also be a factor for accelerating its release from CD–DOX.

In vitro cellular examination of CD–DOX conjugates

For evaluating the cytotoxicity of the as-synthesized carboxyl-rich CDs on liver cell lines, we have selected human liver carcinoma cell lines, namely HepG2 cells, and human normal liver cell lines, namely HL-7702 cells, for comparison. As shown in Fig. 3a and b, both HepG2 cells and HL-7702 cells were cultured from 6 h to 96 h with the medium containing free CDs with the final concentrations ranging from 1.5625 to 100 μg ml^{-1}. The cell viability was measured using sulforhodamine B (SRB) assay. The results showed that there is no influence of the CDs on the viability of cell growth within the investigated CD concentration range. The cell viability kept constant at about 100% compared to the control groups even when the toxicity evaluation duration was extended to 96 h. It is worth noting that in other studies[18,28] where CDs were evaluated

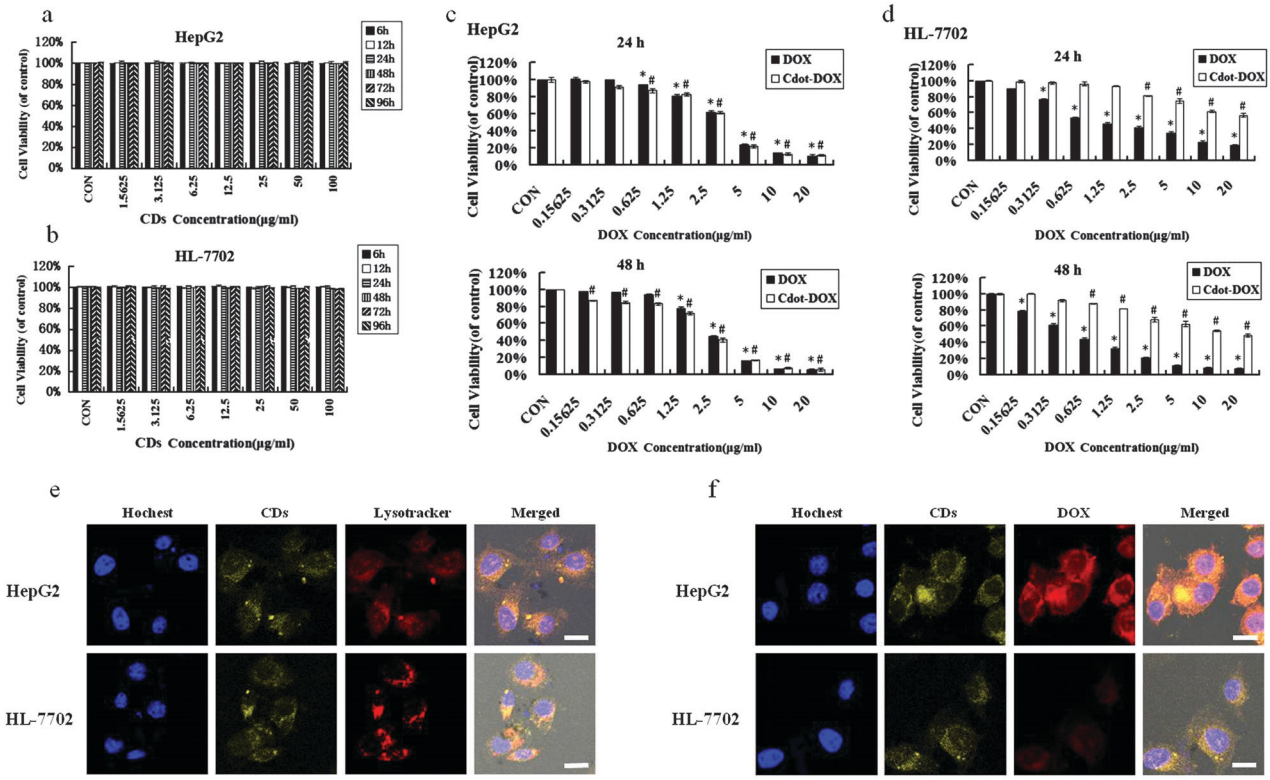

Fig. 3 Cytotoxicity of CDs of different concentrations with HepG2 cells (a) and with HL-7702 cells (b) at different incubation times. Viability of cells after treatment with CDs in DMEM medium at 37 °C in a humidified atmosphere with 5% CO_2. (c) Effect of DOX concentration on the viability of HepG2 cells after co-incubation with DOX and CD–DOX conjugates for 24 and 48 h. When the concentration of DOX reached 2.5 μg ml^{-1}, over 40% HepG2 cells co-incubated with DOX and CD–DOX conjugates were dead. The cytotoxicity of DOX was dose dependent. *$P < 0.01$ *versus* the HepG2 cells co-incubated with DOX drugs; #$P < 0.01$ *versus* the HepG2 cells co-incubated with the CD–DOX conjugates. (d) Effect of DOX concentration on the viability of HL-7702 cells after co-incubation with DOX and CD–DOX conjugates for 24 and 48 h. When the concentration of DOX reached 0.625 μg ml^{-1}, over 40% HL-7702 cells co-incubated with DOX were dead and the survival rate of HL-7702 cells co-incubated with CD–DOX conjugates is close to 100% in contrast. The cytotoxicity of DOX was dose dependent. *$P < 0.01$ *versus* the HL-7702 cells co-incubated with the DOX drugs; #$P < 0.01$ *versus* the HL-7702 cells co-incubated with the CD–DOX conjugates. (e) Endocytosis of CDs observed under confocal microscopy. The blue fluorescence is due to Hoechst for cell nucleus death, the green-yellow fluorescence is from the CDs, and the red fluorescence is from Lysotracker-red for the lysosome. The last column is the overlay of the three micrographs. (f) Endocytosis of CD–DOX and release of DOX in HepG2 and HL-7702 under confocal microscopy. The blue fluorescence is due to Hoechst for cell nucleus death, the green-yellow fluorescence is from the CDs, and the red fluorescence is from the DOX drugs themselves. The last column is the overlay of the three micrographs. The scale bar represents 10 μm.

as low to nontoxic, there was 10–20% growth inhibition and the co-incubation time was usually shorter, typically between 12–48 h. This suggests that the as-synthesized carboxyl-rich CDs are benign to these two cell lines and could be used as a safe fluorescent tracer for DOX release investigation.

Secondly, we evaluated the therapeutic effect of the CD–DOX nanoformulation in comparison to DOX alone in cancerous and normal liver cells. Fig. 3c shows the cytotoxic effect of CD–DOX in cancerous HepG2 cells dosed with DOX and CD–DOX for 24 and 48 h by the SRB assay. The results are presented in percentage of cell viability with respect to control cells. The results show that both DOX and CD–DOX treatments caused dose-dependent death of HepG2 cells with similar trends. The minimum effective concentration of DOX was 2.5 μg ml^{-1} in both systems since over 40% of the cells were dead, and there was no significant cytotoxicity observed at lower concentrations of DOX drug. When the incubation time was prolonged from 24 h to 48 h, more cell death was observed. The similar effectiveness of DOX and CD–DOX in killing HepG2 cells indicates that the two drug formulations have a similar efficacy *in vitro*. However, the cytotoxicity results of cells treated with CDs or CD–DOX in normal hepatic cells, namely HL-7702 cells, were in stark contrast to those in HepG2; as shown in Fig. 3d, the CD–DOX showed almost no toxicity, although the DOX alone is even more effective for killing the HL-7702 cells, requiring only a dosage of 0.625 μg ml^{-1} of DOX for killing 40% of HL-7702 cells. The higher sensitivity of normal cells to the chemotherapy than that of cancer cells may be explained by the multiple drug resistance problem exhibited by cancer cells.[38] This *in vitro* study shows that CD–DOX nanoformulations are highly effective in killing tumor cells, but safe to normal cells, because the DOX can be discriminatively released in cancer cells due to the pH difference.

In order to determine the localization of CDs or CD–DOX nanoformulations in cells and assess the cells' morphological changes, a fluorescence imaging study of HepG2 and HL-7702 cells incubated with CDs and CD–DOX conjugates was performed as shown in Fig. 3e and f, respectively. In Fig. 3e, the CDs are observable in the whole cells after co-incubation in both HepG2 cells and HL-7702 cells. The cell nucleus and lysosomes of both cell lines were labeled with Hoechst (blue) and Lysotracker (red), respectively. The overlay of the images of three channels shows that the CDs and the lysosome overlaid the greatest area in the plasma with orange fluorescence, indicating that most of the intracellular CDs were taken up by the lysosome. Moreover, the morphology of the cells that have uptaken CDs appears to be normal, suggesting that the CDs are a safe cellular fluorescence probe, consistent with the cell viability assay results. The mean fluorescent intensity (MFI) of internalized CDs in both HepG2 and HL-7702 cells was evaluated by flow cytometry to demonstrate their cellular uptake ability. As shown in Fig. S2 (ESI†), the MFIs of HepG2 and HL-7702 cells exposed to CDs for 3 h are similar, which proves the similar amount of cellular uptake of CDs.

To observe DOX release *in vitro*, a similar set of confocal fluorescence images were obtained for HepG2 cells and HL-7702 cells that were co-incubated with CD–DOX for 3 hours. However, in this set of experiments, red-emitting Lysotracker was not applied because of the emission overlap with DOX. As shown in Fig. 3f, the red fluorescence of DOX is only observed in HepG2 cells, but not in the HL-7702 cells. As shown in earlier characterization, the CD–DOX predominantly emits in green in contrast to red-fluorescence free DOX molecules, therefore, such a contrast in Fig. 3f indicates that the bound DOX molecules are released in cancerous HepG2 cells, but not in HL-7702 cells. Furthermore, different to the results of CDs alone (see Fig. S3a, ESI†), HepG2 cells dosed with CD–DOX nanoformulations during incubation showed cell apoptosis such as shrinkage and deformation (see Fig. S3b, ESI†), while HL-7702 cells dosed with CD–DOX presented normal morphology (see Fig. S3c, ESI†), further confirming that CD–DOX selectively damaged the cancer cells. Fig. S3b and c (ESI†) show the morphology of HepG2 cells and HL-7702 cells incubated with 5 μg ml^{-1} CD–DOX, respectively. Compared with the HL-7702 cells, the morphology of HepG2 cancer cells treated with the CD–DOX nanoformulation all showed granular cytoplasm, undefined nuclei, and evidence of blebs during incubation of the drugs. In contrast, the morphology of HL-7702 cells dosed with CD–DOX maintained a healthy appearance, showing no DOX drug effects. The results demonstrated that the CD–DOX nanoformulations are only destructive to tumor cells but are safe to normal cells.

To verify the universality of the CD–DOX drugs to cancer cells, two other cancer cell lines, namely HeLa from human cervical carcinoma and MCF-7 from human breast adenocarcinoma, and two other normal cell lines, namely cardiomyocytes (H9C2) and human umbilical vascular endothelial cells (HUVECs), were also employed for the same set of evaluations. As shown in Fig. S4 (ESI†), there were no differences in the cell viability, which proves again that the CDs prepared by our method were safe to the four cell lines. However, when the DOX alone was injected into the four cell lines, with the increase of the DOX' concentration, the cell viability showed an obvious declining trend, evidencing the therapeutic effect of the DOX drugs. Most noteworthy is that when the CD–DOX nanoformulations were applied to the cancer cells (HeLa (Fig. S4a, ESI†) and MCF-7 (Fig. S4b, ESI†)) and normal cells (H9C2 (Fig. S4c, ESI†) and HUVECs (Fig. S4d, ESI†)), the cell viability results clearly show the selective therapeutic effect of the CD–DOX drugs in cancer cells. This test shows that the targeted therapeutic function of the CD–DOX nanoformulation to cancer cells is universal to all malignant cells that have lower pH compared to normal cells.

In vivo antitumoral activity and biodistribution of the CD–DOX nanoformulation

Since intravenous chemotherapy often leads to severe complications and abandonment of therapy owing to systemic toxicity,[18,39] studies have shown that intratumoral delivery of drugs by direct injection into the tumor mass may provide extremely high drug doses at the target site while minimizing systemic toxicity.[18] Therefore, in this work the intralesional injection of CD–DOX was first used for the treatment of liver cancer of nude white mice. As shown in Fig. 4, the HepG2 tumor sizes in DOX (Fig. 4b) and CD–DOX (Fig. 4c) treated mice are significantly reduced. Whereas when no drug was injected, the volume of the

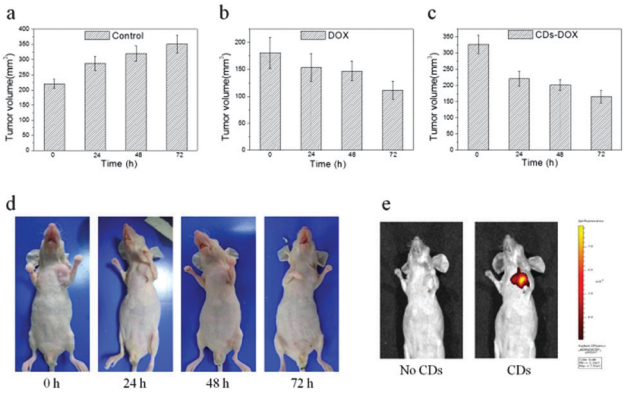

Fig. 4 Tumor sizes of the HepG2 tumor in the BALB/c-nude mouse model: (a) control samples with no drug dose; (b) samples dosed with DOX; (c) samples dosed with CD–DOX conjugates, as a function of time. (d) Photographs of the HCC tumor site after intralesional injection of CD–DOX for different times. (e) *In vivo* fluorescence image of a BALB/c-nude mouse bearing HCC liver cancer before and after intralesional injection of CD–DOX.

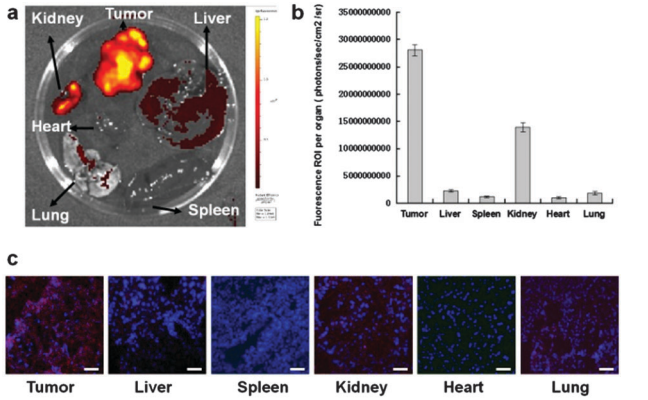

Fig. 5 *In vivo* biodistribution of CD–DOX in HepG2 tumor-bearing mice: (a) distribution of CD–DOX in different organs of HepG2 tumor-bearing mice, taken 24 hours after intravenous administration of CD–DOX and imaged by IVIS. The strength of the fluorescence is shown in the side bar. (b) Biodistributions of CD–DOX in organs based on the fluorescence intensity of the CD signal (n = 3) group. (c) Confocal microscopic imaging of DOX accumulation in tissue sections taken from the tumor, liver, spleen, kidney, heart, and lung, respectively. Scale bars are 100 μm.

tumor monotonically increased with time (Fig. 4a). This result suggests that both DOX and CD–DOX can enter tumor cells to function as antitumor drugs. Fig. 4d shows time-sequenced photographs of a BALB/c-nude mouse treated with CD–DOX drugs, where the reduction of the tumor volume is visible. Fig. 4e shows the fluorescence emission from the tumor site of a mouse injected with CD–DOX in comparison to a mouse without any CDs injected (both under 405 nm line excitation), demonstrating the function of the green-emitting CDs as an *in vivo* fluorescence tracing agent for studying drug biodistribution.

Moreover, the CD–DOX nanoformulation showed improved drug efficacy as displayed in Fig. 4c. After 72 hours treatment, CD–DOX reduced 50% of the tumor volume, while DOX alone reduced 30%. It is also observed that CD–DOX were most effective in the first 24 hours, reducing the tumor volume by 32% in the first 24 hours, suggesting a rapid DOX release of the nanoformulation. The improved efficacy of CD–DOX *versus* DOX may be attributed to the reduced drug resistance of cancer cells to the nanoformulation.

To study the *in vivo* stability and biodistribution of CD–DOX in the mouse body, the whole tumor as well as major organs, such as the liver, spleen, lung, kidney, brain, and heart, were removed 24 h after one-time injection in the tail vein, and *ex vivo* fluorescence images were obtained immediately. As shown in Fig. 5a, the tumor tissue in CD–DOX-treated mice had the highest fluorescence intensity of CD signal compared to the other organs, and the kidney also showed stronger fluorescence intensity of CD signal compared to the other organs. A quantitative analysis of the fluorescence intensity in tumor tissue with CD–DOX using fluorescence spectroscopy (Fig. 5b) shows consistent results with the *ex vivo* fluorescence images. The fluorescence distribution in different organs demonstrated that CD–DOX mainly passively targeted the tumor site by an enhanced permeability and retention (EPR) effect, as well as being accumulated by reticuloendothelial system (RES) organs, such as the liver and spleen. Moreover, cryo-sections of the tumor and organs were prepared and imaged by confocal laser scanning microscopy (CLSM) to analyse the DOX distribution. As shown in Fig. 5c, in CD–DOX-treated HepG2 tumor-bearing mice, the tumor site has the highest DOX accumulation as shown by the strongest red fluorescence, in comparison to other healthy organs such as the liver, spleen, kidney, heart, and lung which show much less or none of the red fluorescence. This shows that the EPR effect plays a dominant role in CD–DOX *in vivo* biodistribution, which is critical for this drug delivery system to achieve localized cancer therapy.

This study also shows that the non-covalent bonding of CD–DOX is reasonably stable in the normal physiological environment. Non-covalent and stimuli-responsive binding between the drug carrier and drug payload is highly desirable for devising drug delivery systems, so that the metabolism of the drug and clearance of the drug carrier can be dealt with separately. The small size of CDs (<10 nm) means that they are very likely to be cleared by renal excretion.[40] More importantly, our previous work[41] systematically evaluated single and repeated dose toxicity of the same CDs in mice, and we demonstrated that none of the CDs exerted any significant toxic effect on mice at the doses used in our experiments. Thus, we believe our CDs will be a safe nanocarrier for *in vivo* fluorescence imaging and anti-cancer drug delivery.

DOX chemotherapy is a unique form of drug delivery system that allows for negative selection of malignant cells using a prodrug approach. It is an exciting strategy currently in clinical trial in the treatment of a number of tumors, such as liver cancer, lung cancer, breast cancer, ovarian cancer, *etc.*[35] However, normal human cells also suffer from this drug due to low selectivity, which potentially may cause long-term organ damage and increased risk of side effects. As a result, it might restrict the application of this promising method. Therefore it is important to develop new strategies for labeling and monitoring DOX in order to kill cancer cells selectively without damaging normal healthy cells.

To solve this problem, we employed CDs as a tool for labeling and monitoring DOX since CDs have high fluorescence intensity and photostability for a long time. The selective drug release from the CD-DOX in the acidic cellular environment of cancer cells has been clearly demonstrated in our *in vitro* and *in vivo* studies. These results indicate that CDs provide a smart drug carrier system in cancer therapy, affording both trackability and targeted release. From the results and analysis above both the tumor inhibition rate of *in vivo* experiments using the BALB/c-nude mouse as the HCC tumor carrier, it can be inferred that electrostatically adsorbed CD–DOX conjugates are very effective and reasonable drugs that could have potential applications in theranostics.

Conclusions

In this study, we have shown that green-emitting CDs synthesized by facile microwave synthesis using citric acid and urea as the precursors can function as a targeted and trackable drug delivery agent for localized cancer treatment in a liver cancer mouse model. The carboxyl-rich CDs are not only non-toxic to a wide range of cell lines, but also provide suitable surface chemistry for forming hydrogen bonds with the $-NH_2$ moiety on the DOX cancer drug, thereby forming CD–DOX drug conjugates. The pH sensitivity of this noncovalent bond serendipitously operates within the pH difference between cancer and normal cells, meaning breaking under mild acidity, *e.g.* pH 5.4 and binding under neutral pH.

The CD–DOX conjugates showed no noticeable negative effect on normal cells, but strong killing effect to cancer cells, demonstrating the targeted drug release effect owing to the sensitivity of the non-covalent bonding to pH and the pH difference between cancer and normal cells. Further *in vivo* study carried out on a liver cancer mouse model demonstrated the suitability of the fluorescent CDs as an *in vivo* bioimaging probe, and more importantly, the stability of such a CD–DOX conjugate in an *in vivo* environment and its enhanced drug efficacy toward cancer cells. The study shows fluorescent CDs are a promising platform that can be engineered into a multifunctional therapeutic agent owing to their rich surface chemistry, nontoxicity and small size.

Experimental section

Chemicals and reagents

Doxorubicin hydrochloride, citric acid, urea and agarose gel were purchased from Sigma-Aldrich. Cell culture media were purchased from Invitrogen. All the reagents were used without further purification. Deionized water was purified through a Milli-Q water purification system with the resistivity of 18.2 MΩ cm.

Synthesis of water-soluble CDs

The microwave synthesis of CDs just followed our previously established procedure.[20] CDs were prepared from urea and citric acid at mass ratios of 2 : 1. First, citric acid (3 g) and urea (6 g) were added to distilled water (10 ml) to form a transparent solution. The solution was then heated in a domestic 650 W microwave oven for 4–5 minutes, during which the solution changed from colorless liquid to brown and finally to a dark-brown clustered solid, indicating the formation of CDs. This solid was then transferred to a vacuum oven and heated at 60 °C for 1 h. The as-prepared CDs were processed in water or ethanol aqueous solution (ethanol volume concentration: 65%), followed by centrifugation (3000 r min^{-1}, 20 min) to remove large or agglomerated particles.

Loading DOX on CDs

As illustrated in Fig. 1, DOX was loaded on CDs by using electrostatic interactions. Firstly, 1 ml of CDs (10 mg ml^{-1}) was mixed with 1 ml of DOX (10 mg ml^{-1}) in phosphate buffer saline (PBS, pH 7.4) with a mass ratio of 1 : 1. The adsorption of DOX on CDs was confirmed by the agarose gel (0.8% w/v) electrophoresis technique. Agarose gel electrophoresis was run at 150 V cm^{-1}, for 10 min. To study the release behavior, 10 mg of CD-DOX were encapsulated into a dialysis bag (molecular weight cut-off 5000) and put into 10 ml of PBS solutions with different pH values (pH = 7.4, 5.0). Then, the releasing process was performed on a shaking table at 37 °C. At timed intervals, the amount of released DOX in the supernatant was measured by PL spectrophotometry at an excitation and emission wavelength of 479 and 591 nm, respectively.

Cell culture and cell uptake

The human hepatocellular carcinoma cell lines (HepG2), human hepatic embryo cell lines (HL-7702), human cervical carcinoma cell line (HeLa), human breast cancer cell line (MCF-7), rat myocardial cell line (H9C2), and human umbilical vascular endothelial cells (HUVECs) were maintained at 37 °C under 5% CO_2 in RPMI-1640 (GIBCO) supplemented with 10% (v/v) heat-inactivated fetal bovine serum (FBS, Invitrogen), penicillin (100 U ml^{-1}), and streptomycin (100 μg ml^{-1}).

HepG2 and HL-7702 cells were seeded on lean coverslips in a 24-well plate at a seeding density of 2×10^4 cells per well. After 24 h, the old medium was discarded. Then, fresh culture without serum and antibiotics were added in the cells. To measure intracellular localization, CDs were co-cultured with HepG2 and HL-7702 cells for 3 h. The cells were then treated with 50 nM LysoTracker Red DND-99 (Invitrogen) for another 1 h, then cells were washed twice again with chilled PBS and the nuclei were stained with Hoechst 33258 (5 μg ml^{-1}) for 5 min. Then the cells were washed twice with PBS. The CD location was observed by confocal laser scanning microscopy. Confocal laser scanning microscopy was carried out using an Olympus FV1000 microscope equipped with a multi-line argon LASER, and a 30 mW Laserclass 3D laser.

Cytotoxicity of CDs, DOX, and CD–DOX nanoformulation

The *in vitro* cytotoxicity of CDs, free DOX, and the CD–DOX nanoformulation against HepG2, HL-7702, HeLa, MCF-7, H9C2 and HUVEC cells was assessed using traditional sulforhodamine B (SRB) assays. The SRB assay is routinely used for cytotoxicity

determination, based on the measurement of live cell protein content. In brief, cells were seeded in 96 well plates at a density of 5×10^3 cells per well overnight, and treated with the indicated different concentrations (100, 50, 25, 12.5, 6.25, 3.125, 1.5625 μg ml^{-1}) of CDs for 6, 12, 24, 48, 72 and 96 h. In another experiment, cells treated with the indicated different concentrations (20, 10, 5, 2.5, 1.25, 0.625, 0.3125 and 0.15625 μg ml^{-1}) of free DOX or CD–DOX nanoformulation at the same DOX concentrations for 24 and 48 h. Afterwards, 100 μl of 20% trichloroacetic acid (TCA) was added to the culture medium in each well and refrigerated at 4 °C for 3 h, then the supernatant was discarded and the plate was washed 5 times with water and air dried. 100 μl of SRB solution 0.4% (w/v) in 1% acetic acid was added to each well and incubated for 30 minutes at room temperature. Unbound SRB was flicked off the plates and the plates were air-dried. Bound SRB was solubilized with 150 μl of 10 mM Tris-HCl to each well and the plate was shaken for 5 minutes.

The cell viability was calculated as a percentage from the viability of the control (untreated) cells. The viability of the control cells was considered as 100%. The results are means ± SE from three independent experiments.

Statistical analysis

Data were expressed as mean ± SD. The statistical significance of the data was compared by Student's *t*-test. Analysis of variance (ANOVA) was used to analyze the differences among the different groups. The results were considered to be significant at $P < 0.05$.

In vivo fluorescence imaging

All animal experiment protocols were approved by the Ethics Committee for the Use of Experimental Animals of Jilin University. Female BALB/c-nude mice (16–20 g, 6–8 weeks of age) were purchased from Beijing HFK Bioscience Co., Ltd and bred in the Center of Experimental Animals of Jilin University under standard pathogen-free conditions. Care and housing were under the supervision of authorized investigators of the local Ethics Committee for Animal Research at Jilin University and in accordance with the international standards for animal welfare. HepG2 cells (2×10^6) were collected in 70 μl PBS and mixed with 70 ml Matrigel Matrix (Becton Dickinson Biosciences). The mixture was injected subcutaneously on one side of the dorsal flank of mice. In *ex vivo* tissue distribution experiments, mice with a HepG2 xenograft after 4 week inoculation were used and treated with CD–DOX conjugates (25 mg kg^{-1}) or free DOX (5 mg kg^{-1}) by a one-time tail vein injection. The mice were sacrificed 24 h post-injection. The tumor and major organs (heart, liver, spleen, lung, and kidney) were removed and imaged by *in vivo* living image analysis (IVIS Spectrum, Caliper Life Sciences, Hopkinton, USA) at an excitation wavelength of 488 nm. Images were collected and analyzed using Living Image 3.1 software (Caliper Life Sciences). Fluorescence intensity at the ROI is expressed as the mean ± SD for three mice in each group. Moreover, all the tissues were immediately frozen and prepared into 4 μm sections, and then the sections were soaked in cold acetone for 3 min, rinsed with PBS for 15 min at room temperature following nuclear staining by Hoechst 33258. Fluorescence visualization of DOX in the tumor and tissues was performed by CLSM. For *in situ* tumor imaging, HepG2 tumor-bearing mice were subcutaneously injected with CD–DOX (10 mg ml^{-1} of Pt, 50 μl) at the center of the tumor after being anesthetized by intraperitoneal injection of 1% pentobarbital. Then mice were imaged by *in vivo* living image analysis (IVIS Spectrum, Caliper Life Sciences, Hopkinton, USA) at an excitation wavelength of 405 nm. Images were collected and analyzed using Living Image 3.1 software (Caliper Life Sciences).

The inhibitory tumor growth effect *in vivo*

HepG2 tumor-bearing mice were prepared for evaluating the *in vivo* antitumoral activity of CD–DOX. When the tumor volume reached 100 mm^3, 18 mice were divided into three groups; 50 μl of the CDs or CD–DOX (10 mg ml^{-1} of Pt) were injected into the center of the tumor in the CDs or CD–DOX group, respectively, while 50 μl PBS was injected into the tumors in the control group. The body weights and tumor sizes were recorded once every one day and the tumor volumes were calculated according to the formula: length × width^2 × 0.52. The mice were sacrificed and imaged at 72 hours after treatment.

Acknowledgements

This work was supported by the National Natural Science Foundation of China (61275197, 61205025, 81225010, and 81371681), the Youth Innovation Promotion Association of CAS (2014194) and the Science and Technology Development Project of Jilin Province under Grant No. 20130206105SF and No. 20150101190JC.

References

1 P. Alivisatos, *Nat. Biotechnol.*, 2004, **22**, 47–52.
2 J. K. Jaiswal, H. Mattoussi, J. M. Mauro and S. M. Simon, *Nat. Biotechnol.*, 2003, **21**, 47–51.
3 L. Y. Liao, J. Liu, E. C. Dreaden, S. W. Morton, K. E. Shopsowitz, P. T. Hammond and J. A. Johnson, *J. Am. Chem. Soc.*, 2014, **136**, 5896–5899.
4 J. Conde, F. R. Tian, Y. Hernandez, C. C. Bao, D. X. Cui, K. P. Janssen, M. R. Ibarra, P. V. Baptista, T. Stoeger and J. M. Fuente, *Biomaterials*, 2013, **34**, 7744–7753.
5 J. Lin, S. J. Wang, P. Huang, Z. Wang, S. H. Chen, G. Niu, W. W. Li, J. He, D. X. Cui, G. M. Lu, X. Y. Chen and Z. H. Nie, *ACS Nano*, 2013, **7**, 5320–5329.
6 J. Conde, C. C. Bao, D. X. Cui, P. V. Baptista and F. R. Tian, *J. Controlled Release*, 2014, **183**, 87–93.
7 S. J. Guo, D. Li, L. X. Zhang, J. Li and E. K. Wang, *Biomaterials*, 2009, **30**, 1881–1889.
8 J. Gautier, E. Allard-Vannier, E. Munnier, M. Souce and I. Chourpa, *J. Controlled Release*, 2013, **169**, 48–61.
9 K. Cheng, S. Peng, C. J. Xu and S. H. Sun, *J. Am. Chem. Soc.*, 2009, **131**, 10637–10644.

10 D. S. Wang, B. W. Fei, L. V. Halig, X. L. Qin, Z. L. Hu, H. Xu, Y. Q. Wang, Z. J. Chen, S. J. Kim, D. M. Shin and Z. Chen, *ACS Nano*, 2014, **8**, 6620–6632.
11 D. Shao, Q. H. Zeng, Z. Fan, J. Li, M. Zhang, Y. L. Zhang, O. Li, L. Chen, X. G. Kong and H. Zhang, *Biomaterials*, 2012, **33**, 4336–4344.
12 D. Shao, J. Li, X. A. Xiao, M. Zhang, Y. Pan, S. Li, Z. Wang, X. Zhang, H. L. Zheng, X. W. Zhang and L. Chen, *ACS Appl. Mater. Interfaces*, 2014, **6**, 11082–11090.
13 X. Q. Yang, J. J. Grailer, L. J. Rowland, A. Javadi, S. A. Hurley, V. Z. Matson, D. A. Steeber and S. Q. Gong, *ACS Nano*, 2010, **4**, 6805–6817.
14 H. J. Zhu, H. B. Chen, X. W. Zeng, Z. Y. Wang, X. D. Zhang, Y. P. Wu, Y. F. Gao, J. X. Zhang, K. W. Liu, R. Y. Liu, L. T. Cai, M. Lin and S. S. Feng, *Biomaterials*, 2014, **35**, 2391–2400.
15 J. Zhao and S. S. Feng, *Biomaterials*, 2014, **35**, 3340–3347.
16 K. Y. Choi, H. Y. Yoon, J. H. Kim, S. M. Bae, R. W. Park, Y. M. Kang, I. S. Kim, I. C. Kwon, K. Choi, S. Y. Jeong, L. Kim and J. H. Park, *ACS Nano*, 2011, **5**, 8591–8599.
17 P. Huang, J. Lin, X. S. Wang, Z. Wang, C. L. Zhang, M. He, K. Wang, F. Chen, Z. M. Li, G. X. Shen, D. X. Cui and X. Y. Chen, *Adv. Mater.*, 2014, **24**, 5104–5110.
18 M. Zheng, S. Liu, J. Li, D. Qu, H. F. Zhao, X. G. Guan, X. L. Hu, Z. G. Xie, X. B. Jing and Z. C. Sun, *Adv. Mater.*, 2014, **26**, 3554–3560.
19 M. L. Chen, Y. J. He, X. W. Chen and J. H. Wang, *Bioconjugate Chem.*, 2013, **24**, 387–397.
20 S. N. Qu, X. Y. Liu, X. Y. Guo, M. H. Chu, L. G. Zhang and D. Z. Shen, *Adv. Funct. Mater.*, 2014, **24**, 2689–2695.
21 S. N. Baker and G. A. Baker, *Angew. Chem., Int. Ed.*, 2010, **49**, 6726–6744.
22 K. Wang, Z. C. Gao, G. Gao, Y. Wo, G. X. Shen and D. X. Cui, *Nanoscale Res. Lett.*, 2013, **8**, 122.
23 Y. P. Sun, B. Zhou, Y. Lin, W. Wang, K. A. S. Fernando, P. Pathak, M. J. Meziani, B. A. Harruff, X. Wang, H. F. Wang, P. J. G. Luo, H. Yang, M. E. Kose, B. L. Chen, L. M. Veca and S. Y. Xie, *J. Am. Chem. Soc.*, 2006, **128**, 7756–7757.
24 S. T. Yang, X. Wang, H. F. Wang, F. S. Lu, P. G. Luo, L. Cao, M. J. Meziani, J. H. Liu, Y. F. Liu, M. Chen, Y. P. Huang and Y. P. Sun, *J. Phys. Chem. C*, 2009, **113**, 18110–18114.
25 K. Hola, Y. Zhang, Y. Wang, E. P. Giannelis, R. Zboril and A. L. Rogach, *Nano Today*, 2014, **9**, 590–603.
26 D. Qu, M. Zheng, J. Li, Z. G. Xie and Z. C. Sun, *Light: Sci. Appl.*, 2015, **4**, e364.
27 C. Q. Ding, A. W. Zhu and Y. Tian, *Acc. Chem. Res.*, 2014, **47**, 20–30.
28 Q. Li, T. Y. Ohulchanskyy, R. L. Liu, K. Koynov, D. Q. Wu, A. Best, R. Kumar, A. Bonoiu and P. N. Prasad, *J. Phys. Chem. C*, 2010, **114**, 12062–12068.
29 R. L. Liu, D. Q. Wu, S. H. Liu, K. Koynov, W. Knoll and Q. Li, *Angew. Chem., Int. Ed.*, 2009, **48**, 4598–4601.
30 J. Tang, B. Kong, H. Wu, M. Xu, Y. C. Wang, Y. Wang, D. Y. Zhao and G. F. Zheng, *Adv. Mater.*, 2013, **25**, 6569–6574.
31 S. Hu, A. Trinchi, P. Atkin and I. S. Cole, *Angew. Chem., Int. Ed.*, 2015, **54**, 2970–2974.
32 H. U. Lee, S. Y. Park, E. S. Park, B. Son, S. C. Lee, J. W. Lee, Y. C. Lee, K. S. Kang, M. Kim, H. G. Park, S. Choi, Y. S. Huh, S. Y. Lee, K. B. Lee, Y. K. Oh and J. Lee, *Sci. Rep.*, 2014, **4**, 4665.
33 C. L. Li, C. M. Ou, C. C. Huang, W. C. Wu, Y. P. Chen, T. E. Lin, L. C. Ho, C. W. Wang, C. C. Shih, H. C. Zhou, Y. C. Lee, W. F. Tzeng, T. J. Chiou, S. T. Chu, J. S. Cang and H. T. Chang, *J. Mater. Chem. B*, 2014, **2**, 4564–4571.
34 R. O. Hynes, *Cell*, 2002, **110**, 673–687.
35 F. H. Chen, Q. Gao and J. Z. Ni, *Nanotechnology*, 2008, **19**, 165103.
36 T. H. Kim, H. W. Ho, C. L. Brown, S. L. Cresswell and Q. Li, *Anal. Methods*, 2015, **7**, 6869.
37 E. Aznar, R. Casasus, B. G. Acosta, M. D. Marcos, R. M. Martinez, F. Sancenon, J. Soto and P. Amoros, *Adv. Mater.*, 2007, **19**, 2228–2231.
38 V. S. Donnenberg and A. D. Donnenberg, *J. Clin. Pharmacol.*, 2005, **45**, 872–877.
39 F. Celikoglu, S. I. Celikoglu and E. P. Goldberg, *Cancer Ther.*, 2008, **6**, 545–552.
40 H. S. Choi, W. Liu, P. Misra, E. Tanaka, J. P. Zimmer, B. I. Ipe, M. G. Bawendi and J. V. Frangioni, *Nat. Biotechnol.*, 2007, **25**, 1165.
41 X. Zheng, D. Shao, J. Li, Y. Song, Y. Chen, Y. Pan, S. Zhu, B. Yang and L. Chen, *RSC Adv.*, 2015, **5**, 91398–91406.

